Nearfield RCS Measurements of Full Scale Targets Using ISAR

Larsson, Christer

Published in:
AMTA Proceedings

2014

Nearfield RCS Measurements of Full Scale Targets Using ISAR

Christer Larsson
Saab Dynamics
581 88 Linköping, Sweden
and
Department of Electrical and Information Technology
Lund University
P.O. Box 118, 221 00 Lund, Sweden
Christer.Larsson@eit.lth.se

***Abstract*—Nearfield Radar Cross Section (RCS) measurements and Inverse Synthetic Aperture Radar (ISAR) processing are used in this study to obtain geometrically correct images and farfield RCS. The back projection algorithm is used to determine the amplitudes and locations for the scatterers in a point by point imaging process. Different approximations are used to sum the nearfield RCS recorded at an azimuthal interval of angles when forming the farfield image. The images obtained show the geometrically correct locations of the target scatterers with exceptions for some target features *e.g.*, when there are multiple or resonance scattering features. Separate features in the images are gated and an inverse processing step is performed to obtain the farfield RCS of the full target or selected parts of the target. Examples of images and farfield RCS extracted from simulations and measurements on small and full scale targets using the ISAR processing techniques described in this paper are given.**

I. Introduction

The definition of the Radar Cross Section (RCS) is based on that the target is illuminated with a planar electromagnetic field, *i.e.*, that the target is at infinite distance from the radar. The question when performing a measurement is then: When is the target far enough from the radar so that the requirement given above is at least approximately true? This distance is given by the commonly used but arbitrary farfield criterion [1],

$$r > \frac{2d^2}{\lambda}, \tag{1}$$

where r is the distance from the radar antenna to the target, d is the size of the target and λ is the wavelength. However, many RCS measurements are performed at distances shorter than those given by (1) due to practical reasons such as cost or available RCS measurement ranges.

There are different strategies employed to handle this dilemma. One is to investigate if the data can be used for some application even when it is recorded at distance shorter than those given by (1). In [2] it is shown that the nearfield measurements can give results similar to farfield results if the data is low pass filtered. Similar conclusions are made in [3] where the authors show that if a cumulative measure is desired it can be taken directly from the nearfield data which provides an upper bound for the cumulative farfield RCS.

It is possible to get a correct transformation to the farfield by using bistatic RCS measurements in the nearfield. This is shown in [4]. This method will in general be very time consuming due to the many sample points that have to be recorded. Another method is to use RCS measurements on a target with known RCS to determine how to convert from the nearfield to farfield [5].

The focus in the present study is on image based methods where images are generated. The purpose of the images is to be an aid in RCS diagnostics where different scattering features in an image are used to analyze the contribution of that features to the total RCS of the target.

One approach to image based extraction of the farfield RCS is to use the same angular interval from the data regardless of the distance to the origin to make ISAR images. This method will work well for RCS extraction when the azimuth angle is close to the center angle of an ISAR image. The procedure is then to only use center angles and to generate a series of ISAR images to use for extraction of the RCS through image gating [6], [7]. We will call this method the "NF-FF" method.

The method can be refined considering parallax, *i.e.*, select which part of the recorded data that should be used on a pixel by pixel basis [8], [9]. The processing time will be longer than for the NF-FF method due to the image point by point selection of the angular interval. We will call this method the "Full NF-FF" method.

An alternative image based approach that does not require the intermediate step of generating images is developed in [10]. The algorithms are shown to give very good performance.

The purpose of the present paper is to analyze the differences between the NF-FF and the Full NF-FF methods using some typical examples of RCS data.

II. Theory

The following description is restricted to a 2D case, *i.e.*, it is assumed that there is a cylindrical wave front impinging on the target. This approximation can be considered quite accurate when the target is smaller in it's vertical than in it's horizontal dimensions, which is often the case. It is also straightforward

to generalize the procedure to a 3D geometry if such data is available.

The measurement is performed by placing the target on a turntable. Calibration of amplitude and phase is done positioning the phase zero at the turntable center. RCS data is obtained by sweeping a range of discrete frequencies while running the turntable and taking care to meet the sampling criterion. This results in a complex valued RCS data set that is used to process ISAR images using a back projection algorithm. The used coordinate system is fixed with respect to the turntable.

The reflectivity distribution function $\psi(x,y)$ at the image coordinates (x,y) is given by

$$\psi(x,y) = \frac{1}{f_\mathrm{c}} \sum_{\varphi_\mathrm{m}\in\Phi} \sum_{\mathrm{n}=1}^{\mathrm{N}} KJA(f_\mathrm{n},\mathrm{m}) \mathrm{e}^{(-\mathrm{i}2k_\mathrm{n}\Delta r_\mathrm{m}(x,y))} f_\mathrm{n}, \quad (2)$$

where the sums are performed over the antenna positions that are inside the relevant angular interval, Φ, for the point (x,y) and N frequencies. $A(f_\mathrm{n},\mathrm{m})$ is the measured radar cross section complex valued amplitude for specific polarizations. $A(f_\mathrm{n},\mathrm{m})$ is related to the measured RCS at frequency f_n and antenna position m, $\sigma(f_\mathrm{n},\mathrm{m})$, by $\sigma(f_\mathrm{n},\mathrm{m}) = |A(f_\mathrm{n},\mathrm{m})|^2$. k_n is the free space wavenumber at frequency f_n, *i.e.*, $k_\mathrm{n} = 2\pi f_\mathrm{n}/\mathrm{c}_0$ where c_0 is the speed of light. $\Delta r_\mathrm{m}(x,y) = (r_\mathrm{m}(x,y) - r_0)$. $r_\mathrm{m}(x,y)$ is the distance from antenna position m to the image point at (x,y) and r_0 is the distance from the antenna to the image origin. $K = K_\mathrm{m}(x,y)$ is a normalization constant that corrects for the distance dependence of the signal received from different parts of the imaged region. $K_\mathrm{m}(x,y)$ is given by

$$K_\mathrm{m}(x,y) = \left(\frac{1}{\mathrm{N}}\right)\left(\frac{r_\mathrm{m}(x,y)}{r_0}\right)^2. \quad (3)$$

$J = J_\mathrm{m}(x,y)$ is a normalization constant that corrects for the step lengths in azimuth as seen from the point (x,y). It is given by

$$J_\mathrm{m}(x,y) = \left(\frac{\delta\varphi_m(x,y)}{\Phi(x,y)}\right), \quad (4)$$

where $\delta\varphi_m(x,y)$ is the angle step with respect to the point (x,y). Equation (2) is basically a discrete version of an expression for $\psi(x,y)$ given in [11].

The difference between the NF-FF and the Full NF-FF method shows up in J. The same angle steps, $\delta\varphi$, and angular interval from the data, Φ, are used for all points in the image in the NF-FF method. In contrast, both the angle steps, $\delta\varphi$, and the angular interval that are used for the processing is adapted to each point in the image for the Full NF-FF method, *i.e.*, $\Phi = \Phi(x,y)$. This is shown schematically in Fig. 1. Different points using the same angular width, $\Delta\varphi$, for the Full NF-FF processing utilize different parts, Φ, of the RCS data set. $\Phi_1 > \Phi_0 > \Phi_2$ in Fig. 1 due to different distances to the radar.

Geometrically correct images can be obtained by performing the summations in (2) for each image point. A faster way is to calculate a downrange profile for each antenna position from the frequency sweep using a fast fourier transform (FFT).

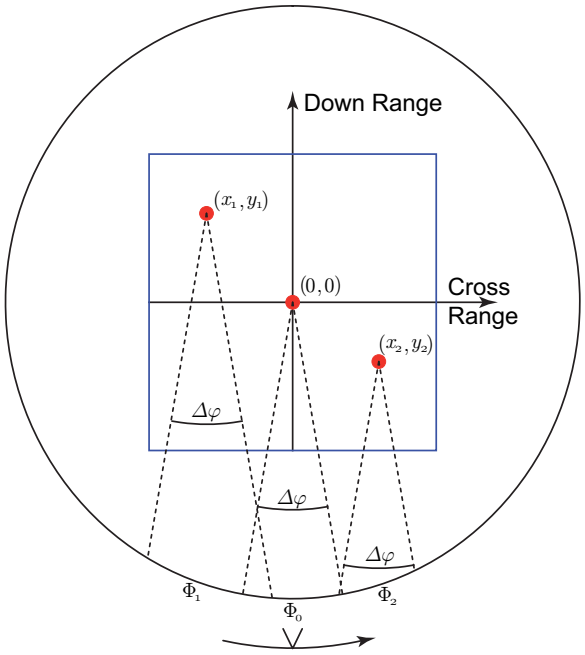

Fig. 1. The figure shows schematically the angular intervals that are needed from the data set in order to get the same angular interval for points at different positions.

The downrange profiles are then used for interpolation and summed together coherently to get the combined reflectivity distribution $\psi(x,y)$ at the image coordinates (x,y) [11].

Image gating can be performed to obtain the farfield RCS for parts of an image. The farfield RCS inside a gate can be obtained by summing the complex valued function ψ coherently inside the gate area, G. This can be expressed as

$$\sigma_\mathrm{G}(f_n,\varphi_m) = L \sum_{x,y\in\mathrm{G}} \psi(x,y)\mathrm{e}^{\mathrm{i}2k_\mathrm{n}\Delta r_m(x,y)}, \quad (5)$$

where L is a normalization constant. L can be determined by processing an image for a synthetic isotropic scatterer with σ=1 m^2 and gating it, thereby obtaining the normalization.

III. Results and Discussion

A. Isotropic Point Scatterers

ISAR images of isotropic point targets with $1\,\mathrm{m}^2$ RCS positioned at $(0,-3)$, $(0,0)$ and $(0,3)$ with $r_0 = 4\,\mathrm{m}$ are shown in Fig. 2. The images in the left and right columns are processed using the NF-FF and the Full NF-FF methods, respectively. The yellow sectors show the intervals of angles that are used for each image. The 6–16 GHz frequency range is used for all images. 45.6° angular width, centered on 0°, is needed to match the cross-range and down-range resolutions assuming that the radar is far away from the target.

This interval of angles from the data is used for the NF-FF method in the left column regardless of the offset distance. The constant angular interval results in a cross-range resolution that varies with the distance between the point target and the radar.

The angular interval that is used for the processing is adapted to the distance to the radar for the Full NF-FF images of the point targets shown in the right column. 14.8°, 48.4° and 82.4° angular interval is used for the images showing the point sources at (0,−3), (0,0) and (0,3), respectively. The widths corresponds to a point by point angular width of 45.6°. This results in a resolution that does not change with distance.

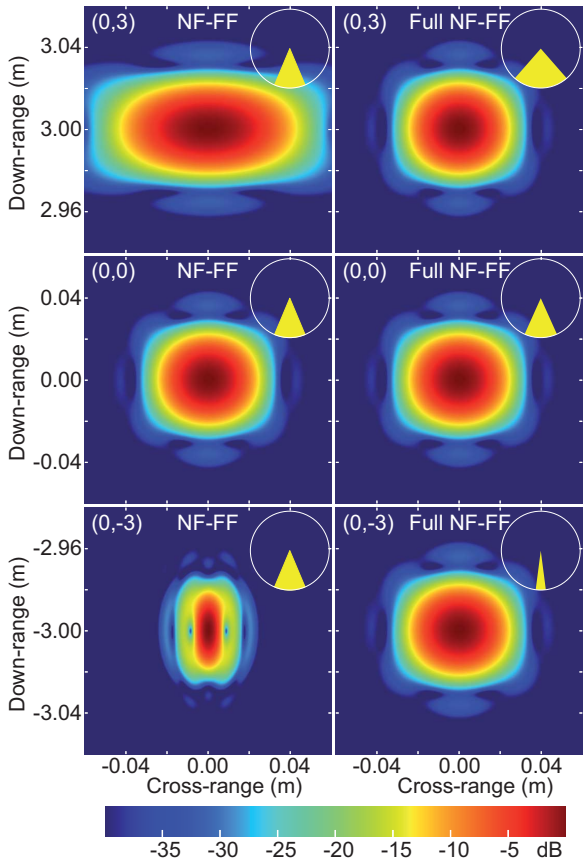

Fig. 2. The images show isotropic point targets positioned at (0,−3), (0,0) and (0,3) with $r_0 = 4$ m. The left and right columns are processed using the NF-FF and Full NF-FF methods, respectively. A Hanning window is used. The filled circle sectors show the part of the angle interval that are used for the images.

Image gating is performed on the complex valued data corresponding to the images in Fig. 2. The resulting RCS for the point targets at (0,−3) and (0,3) are shown in Fig. 3. The Full NF-FF method gives an accurate result for a large part of the angular interval.

The NF-FF method gives large deviations from the correct result. However, it turns out that the cross-range resolution and hence the area of the image of the point and the summed amplitudes is proportional, in first order, to the distance to the radar. The summed intensity then has to be corrected by dividing with $(r_m/r_0)^2$, *e.g.*, for $\varphi = 0°$ subtracting by −12.1 dB and 4.9 dB for the points at (0,−3) and (0,3), respectively. This means that the NF-FF method can be used for the central part of the angles that are used for the processing to aquire farfield RCS using a correction factor.

This means that the NF-FF procedure works best for small offsets from the origin and for the central angles used to make one image. This means that a series of images have to be utilized to get the farfield RCS for a larger angular region. [6], [7]

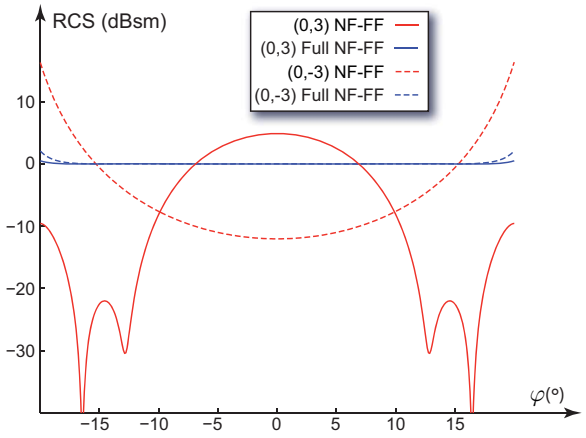

Fig. 3. RCS at $f = 11$ GHz as a function of azimuth angle, φ, extracted from the complex valued data corresponding to the images in Fig. 2 for the point targets at (0,−3) and (0,3). Results are shown for the NF-FF and the Full NF-FF method

B. Measurements of a Metal Cylinder

A measurement on a metal cylinder with length 500 mm and 16 mm radius is performed to investigate some of the effects of measuring at short distance and what effects the different processing methods have on the extracted RCS. The cylinder is positioned at the turntable center, the origin, with the distance to the radar antenna $r_0 = 7.6$ m. The 6–16 GHz frequency range and VV polarization is used for the experiment in an anechoic chamber. A Hanning window is used. The measurement distance is too short to meet the farfield criterion in (1), *i.e.*, that the distance should be larger than 10 and 27 m for 6 and 16 GHz, respectively for this 500 mm wide target.

Fig. 4 shows the resulting ISAR images. The top image is processed assuming infinite distance and using 45.6° angular width. The image of the cylinder is bent compared to the overlay of the cylinder that is placed at the correct position of the object.

The middle image is processed using the NF-FF method using the correct distance to the radar and using 45.6° angular width from the RCS data for all image points. The image is now parallel with respect to the overlay and in the correct geometrical position. However, a small intensity variation is visible in the cross-range.

The bottom image is processed using the Full NF-FF method using the correct distance to the radar and using 52.3° angular width from the RCS data for the image. A point by point angular width of 45.6° is used. The image is similar to the image for the NF-FF method but has no intensity variation with cross-range.

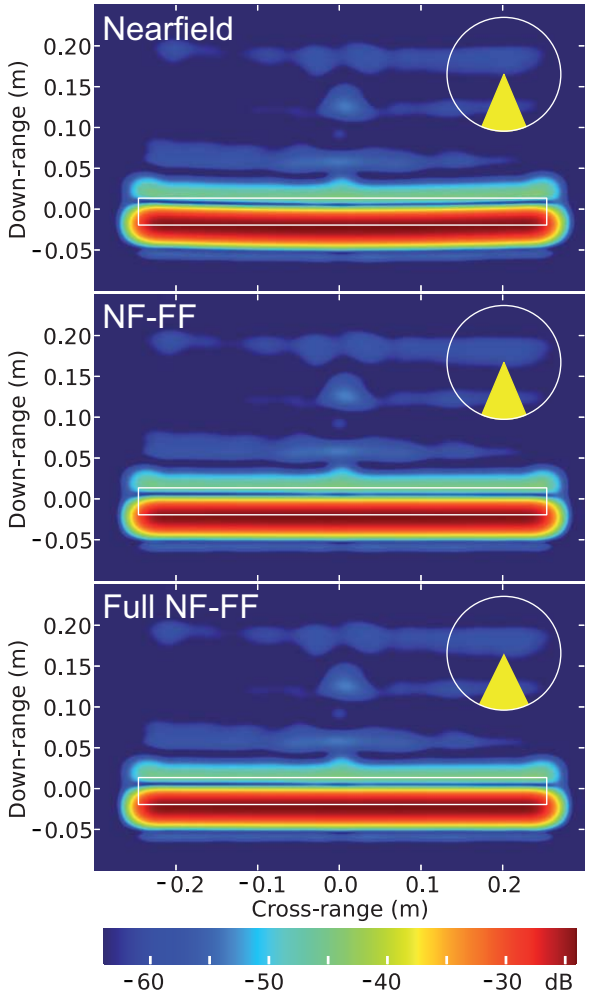

Fig. 4. The images show a measurement of a cylinder positioned at the turntable center, the origin, with $r_0 = 7.6\,\text{m}$. The top image is processed assuming infinite distance, the middle image using the NF-FF method and the bottom image the Full NF-FF method. The angular interval is at 0°. A Hanning window is used for all images. The filled circle sectors show the part of the angle interval that are used for the images.

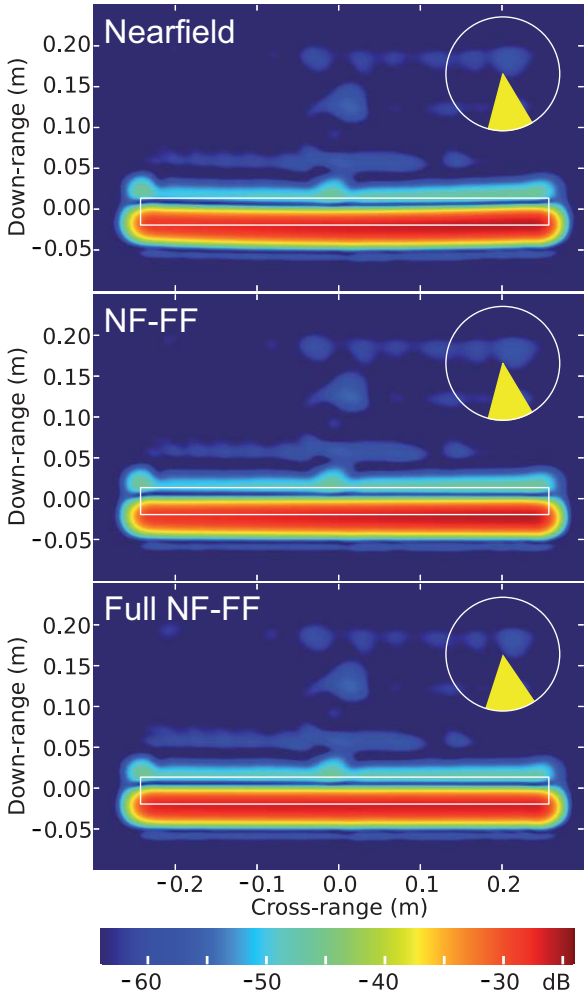

Fig. 5. The images show a measurement of a cylinder positioned at the turntable center, the origin, with $r_0 = 7.6\,\text{m}$. The top image is processed assuming infinite distance, the middle image using the NF-FF method and the bottom image the Full NF-FF method. The angular interval is centered at +8°. A Hanning window is used for all images. The filled circle sectors show the part of the angle interval that are used for the images.

The intensity differences between the NF-FF and Full NF-FF images are investigated in detail by changing the center angle to +8°. These images are shown in Fig. 5. They are processed in the same way as the images in Fig. 4. The intensity variation is now easier to see as it increases from left to right in the NF-FF image in the middle. The Full NF-FF image has an even intensity in the cross-range direction for this center angle also.

This is shown more clearly in Fig. 6 which shows the same data as Fig. 5 but with a smaller dynamic range.

Image gating is performed on the complex valued data corresponding to the images in Fig. 4. The resulting RCS graphs are shown in Fig. 7. Both the NF-FF and Full NF-FF methods give results typical for a cylinder in the farfield for a large part of the angular interval while the RCS that is processed assuming infinite distance is smeared out due to the nearfield with a lower amplitude in the specular direction. It is clear that that some nearfield to farfield processing is needed even for this relatively small object if one requires accurate RCS data.

C. Measurements of a Full Scale Target

Measured X-band data from a full scale target is used to further evaluate the different methods to process the data. Measured data from a STANDCAM (Standard Decoy for Camouflage Materials) is used for this purpose, see Fig. 8. The non-classified target is developed by WTD 52, Oberjettenberg, Germany and is made from metallized glass-fiber reinforced plastic. The right side is wheeled and the left side is tracked in order to simplify comparisons between the two alternatives.

Fig. 9 shows data processed using the previously described methods to process data. The measurement was performed in the 9.25–10.75 GHz frequency range with HH polarization on the right, wheeled side. The distance between the measurement radar and the target was $r_0 = 101\,\text{m}$. For this 5 m wide target

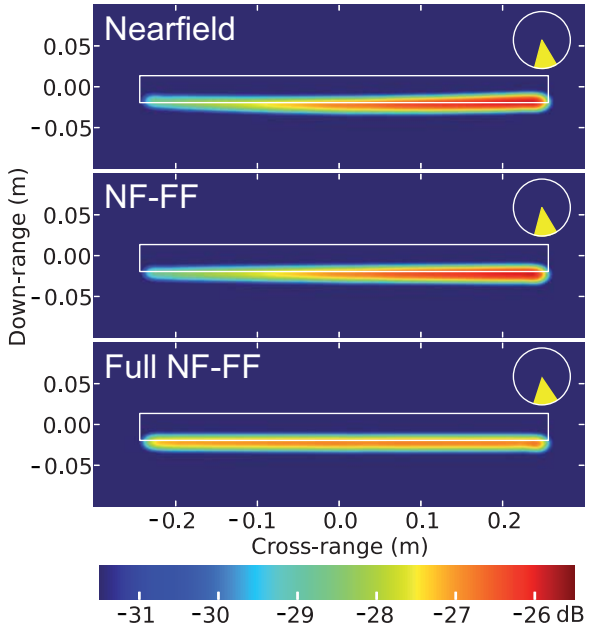

Fig. 6. The figure show the same data as Fig. 5 with a different part of the intensity range.

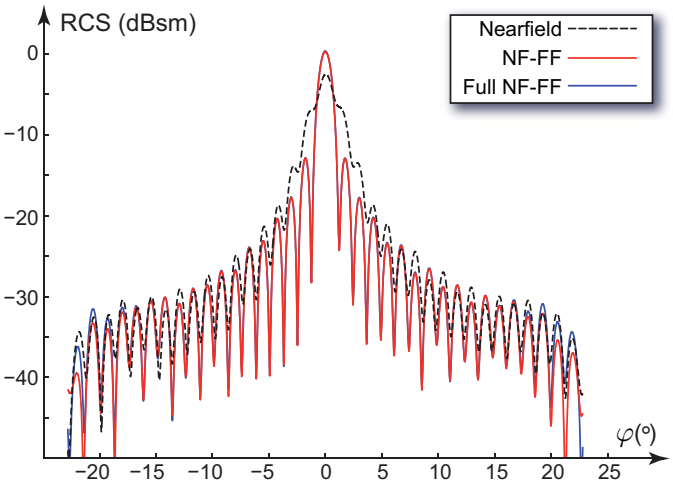

Fig. 7. RCS at $f = 11\,\text{GHz}$ as a function of azimuth angle, φ extracted from the complex valued data corresponding to the images in Fig. 4. Results are shown assuming infinite distance to the target, using the NF-FF method and the Full NF-FF method.

the distance has to be more than 1.7 km for it to be in the farfield according to to (1).

The top image is processed assuming infinite distance and using 5.9° angular width. The image has some very small geometrical distorsions due to the assumption of a planar impinging wave front on the target.

The middle image is processed using the NF-FF method using the correct distance to the radar and using 5.9° angular width from the RCS data for all image points. The image has no distorsion with respect to the overlay and is in the correct geometrical position.

The bottom image is processed using the Full NF-FF method using the correct distance to the radar and using 9.5° angular width from the RCS data for the image. A point by point angular width of 5.9° is used. The image is very similar to the image for the NF-FF method.

Fig. 8. The STANDCAM test target. The right side is wheeled and the left side is tracked.

Image gating is performed on the complex valued data corresponding to the images in Fig. 9. The resulting RCS graphs are shown in Fig. 10. There is good agreement between the NF-FF and Full NF-FF method in the interval $[1°, +1°]$. There are discrepancies between the two methods outside this interval. Furthermore, the NF-FF method results show oscillations with a longer period than for the Full NF-FF period. This is due to that the target is not fully illuminated at angles outside this interval for the selection of data used for the NF-FF method.

IV. Summary and Conclusions

The images obtained using both the NF-FF and the Full NF-FF methods show the geometrically correct locations for the target scatterers with exceptions for some target features *e.g.*, when there are multiple or resonance scattering features.

The NF-FF method will, in general, give good results for the farfield RCS for angles close to the center of the azimuth processing window. A correction factor has to be used to correct for the distance difference to the origin.

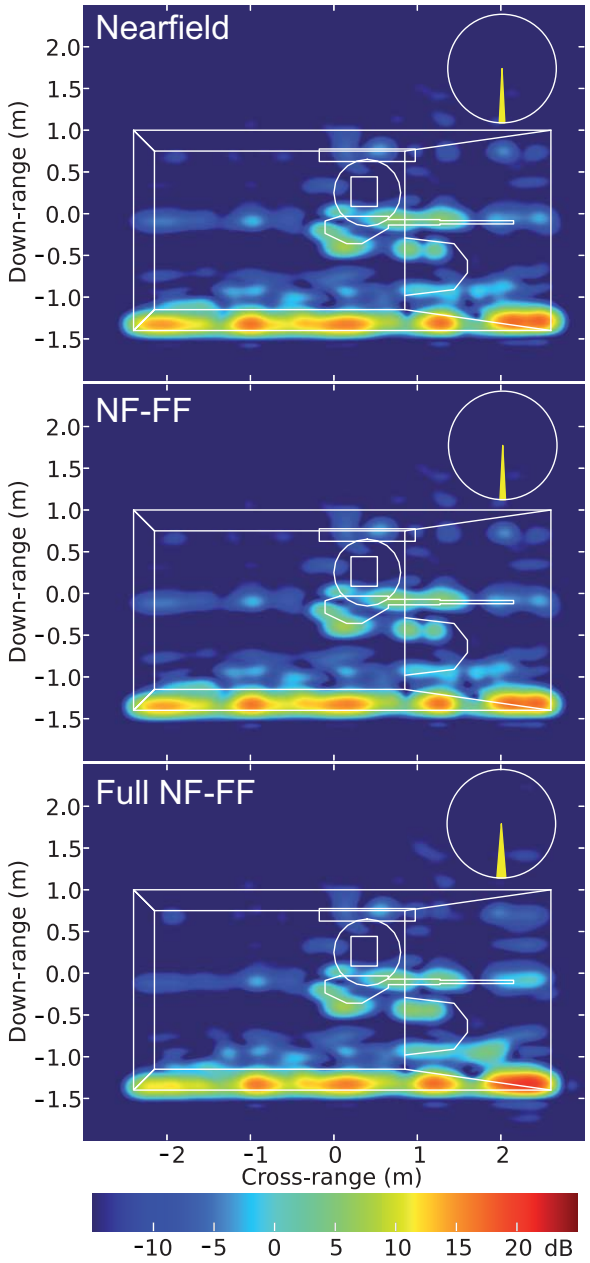

Fig. 9. The images show a measurement of the right, wheeled side of the STANDCAM target positioned at the turntable center, the origin, with $r_0 = 101$ m. The top image is processed assuming infinite distance, the middle image using the NF-FF method and the bottom image the Full NF-FF method. The angular interval is centered at 0°. A Hanning window is used for all images. The filled circle sectors show the part of the angle interval that are used for the images.

The Full NF-FF method will give good results for the farfield RCS without using any correction factor. In fact, given the ISAR image processed with the Full NF-FF method it is not necessary to know the distance that was used in the measurement.

Compensation for the geometry and moving the scattering features to the proper positions is the most important step in the processing methods. Compensation for parallax which is done in the Full NF-FF method is often of less importance but is crucial if the object, or parts of the object are far away from the origin.

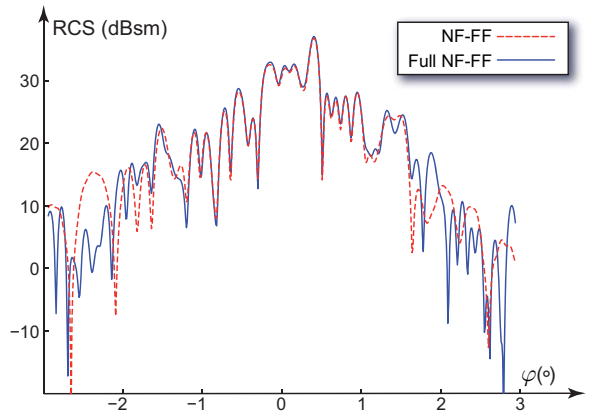

Fig. 10. RCS at $f = 10$ GHz as a function of azimuth angle, φ, extracted from the complex valued data corresponding to the images in Fig. 9. Results are shown for the NF-FF and Full NF-FF methods.

ACKNOWLEDGEMENT

The financial support by the Swedish Defence Materiel Administration is gratefully acknowledged. I would also like to thank Dr. Johan Jersblad at Saab Barracuda for the STANDCAM data and Ms Karin Brage at Saab Dynamics for technical assistance.

REFERENCES

[1] E. F. Knott, J. F. Shaeffer, and M. T. Tuley, *Radar Cross Section*. 5601 N. Hawthorne Way, Raleigh, NC 27613: SciTech Publishing Inc., 2004.

[2] J. O. Melin, "Measuring radar cross section at short distance," *IEEE Trans. Antennas Propagat.*, vol. 35, no. 8, pp. 991–996, Aug. 1987.

[3] M. Naor, V. Kobrinsky, and R. Mizrachi, "Exoneration of performing total RCS measurements in the near field," in *Proc. Antenna Measurement Techniques Association (AMTA)*, Atlanta, GA, 2010, pp. 1–6.

[4] O. M. Bucci and M. D. Migliore, "Effective estimation of 2-D monostatic radar cross sections from near-field measurements," *IEEE Trans. Antennas Propagat.*, vol. 54, no. 2, pp. 750–752, Feb. 2006.

[5] C. R. Birtcher, C. A. Balanis, and V. J. Vokurka, "RCS measurements, transformations, and comparisons under cylindrical and plane wave illumination," *IEEE Trans. Antennas Propagat.*, vol. 42, no. 3, pp. 329–334, March 1994.

[6] J. W. Odendaal and J. Joubert, "Radar cross section measurements using near-field radar imaging," *IEEE Trans. Instrumentation and Measurement*, vol. 45, no. 6, pp. 948–954, Dec. 1996.

[7] H.-O. Berlin, J. Rahm, and C. Larsson, "Columbus – an ISAR navigator," in *Proceedings Antenna Measurement Techniques Association (AMTA)*, Philadelphia, PA, 2000, pp. 75–80.

[8] G. A. Showman and M. A. Richards, "Algorithms for high-precision two-dimensional ISAR imaging on an outdoor turntable range," in *Proc. Antenna Measurement Techniques Association (AMTA)*, Philadelphia, PA, 2000, pp. 69–74.

[9] L. E. Sheffield, "Near-field to quasi-far-field transform through parallax," in *Proc. Antenna Measurement Techniques Association (AMTA)*, Boston, MA, 2008, pp. 1–6.

[10] S. A. Rice and I. J. LaHaie, "A partial rotation formulation of the circular near field-to-far field transformation (CNFFFT)," in *Proc. Antenna Measurement Techniques Association (AMTA)*, Austin, TX, 2006, pp. 1–6.

[11] T. Vaupel and T. F. Eibert, "Comparison and application of near-field ISAR imaging techniques for far-field radar cross section determination," *IEEE Trans. Antennas Propagat.*, vol. 54, no. 1, pp. 144–151, Jan. 2006.